Modelling the neutral density in the edge of the DIII-D plasma

2000 Nucl. Fusion 40 965

(http://iopscience.iop.org/0029-5515/40/5/309)

Modelling the neutral density in the edge of the DIII-D plasma

W.M. Stacey
Fusion Research Center, Georgia Institute of Technology,
Atlanta, Georgia, United States of America

Abstract. A computationally efficient modelling procedure for the calculation of neutral atom densities in the plasma edge is described and applied to calculate the recently measured neutral densities in DIII-D. The agreement of the calculated and measured neutral densities in the plasma edge inside the separatrix is quite good. The implications of these results for neutral transport in the plasma edge are discussed.

1. Introduction

A modelling procedure has been developed for the computationally efficient calculation of neutral particle densities and reaction rates in the plasma edge and divertor of the DIII-D tokamak [1, 2]. This procedure encompasses a simple but comprehensive coupled core-plasma–divertor/SOL-plasma–recycling/fuelling-neutrals calculation [3, 4], together with the systematic use of selected experimental parameters. Although various aspects of the modelling procedure (e.g. the neutral particle calculation for a given edge and divertor plasma background) have been checked by comparison with more detailed calculations, it has not heretofore been possible to compare the neutral density predictions resulting as a consequence of this modelling procedure with direct measurements of the neutral density in the DIII-D edge plasma.

However, a novel method of measuring the neutral density in the plasma edge near the X point has recently been applied in DIII-D [5]. This measurement uses a 2-D reconstruction of D_α light from a tangentially viewing TV camera [6] and the lower, or 'divertor, Thomson scattering measurements to infer neutral densities both above and below the X point. These measurements have been successfully modelled using a 2-D plasma fluid code and a Monte Carlo neutrals calculation [7].

The purpose of this article is to report a comparison of the neutral densities in the DIII-D edge plasma predicted by our computationally efficient procedure with the measured data and with the predictions of the more detailed 2-D fluid plasma/Monte Carlo neutrals modelling procedure. Our modelling procedure is outlined in Section 2, and described in more detail in the Appendixes. The experiment is briefly described and the results of the analysis are presented in Section 3. Implications of the results are discussed in Section 4.

2. Neutral density modelling procedure

The neutral density modelling procedure is built around a computationally economical calculation of the coupled core-plasma–SOL/divertor plasma–recycling/fuelling-neutrals balance equations, supplemented by the systematic use of selected experimentally determined parameters to ensure the fidelity of certain important aspects of the calculation.

2.1. Neutral particle transport model

The mathematical formalism of the interface current balance (ITB) and transmission/escape probabilities (TEP) transport methodology is summarized in Appendix A. With reference to Fig. 1, neutral particle transport is calculated in the outer half of a lower single null divertor configuration by first dividing the region within the plasma and divertor chamber into a small number of regions. The neutral transport in the 'outer' regions — encompassing the divertor plasma leg (D), a small 'recycling' region (R) in which the plasma ions and neutrals incident on the divertor plate are recycled as atoms and molecules, the 'private flux' (PF) region between the two legs of the divertor, the 'plenum' (PL) region at the bottom of the chamber and an upper 'SOL plenum' (SPL) region — is modelled using the TEP methodology [8] of balancing partial currents across interfaces of rather large regions and making use of transmission and escape probabilities to calculate these partial currents. The neutrals current into the pumping duct, located in the lower right hand corner of

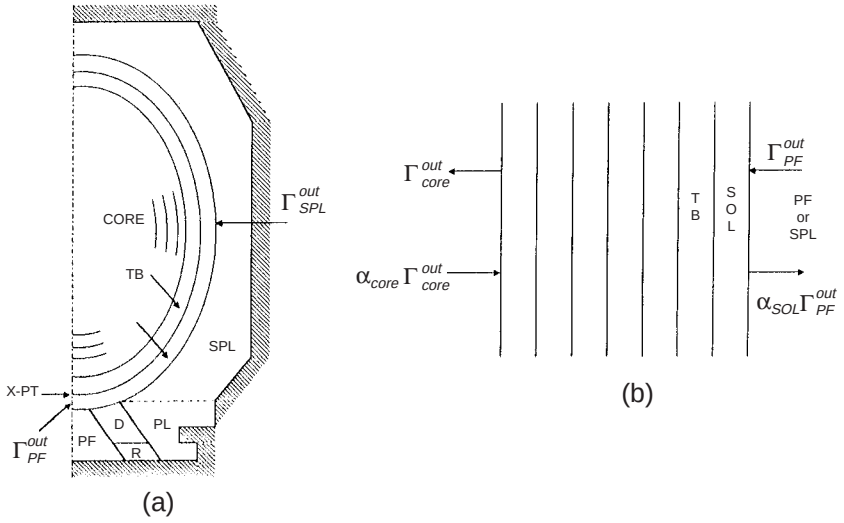

Figure 1. Schematic diagram of the neutral transport model: (a) 2-D TEP model of divertor plasma (D), recycling region (R), private flux (PF), plenum (PL) and SOL plenum (SPL); (b) 1-D ICB model of penetration through SOL and transport barrier (TB) into core.

Fig. 1(a) under the baffle ring, is calculated in terms of the solid angle seen by neutrals emerging isotropically from the D and R regions, thus accounting for the measured separatrix strike point location. The measured separatrix strike point and X point locations are used to calculate the angle of incidence of the recycling ions. The outer bounding material surfaces (including the pump duct when closed) reflect incident ions and neutrals as atoms or re-emit them as molecules. The molecules undergo dissociation and constitute volumetric sources of neutrals and ions to the adjacent region. The inner bounding surface of these 'outer' regions — the interface with the SOL — reflects neutrals with an albedo coefficient α_{sol}. The symmetry surfaces at the left hand boundary of Fig. 1 are assumed to perfectly reflect incident neutrals.

One dimensional neutral 'penetration' calculations of the neutral partial current incident on the SOL are made at the midplane and at the X point using the interface current balance (ICB) methodology [9]. The incident flux for the midplane calculation is the exiting flux from the SPL region into the SOL, and the incident flux at the X point is the exiting flux from the PF region into the SOL at the bottom of the plasma. For the purpose of the neutral penetration calculation, the experimentally measured SOL plasma density and temperature are used. The 'penetration' calculations proceed inwards across the SOL, across the separatrix, across the transport barrier and about 15 cm into the plasma core, where a diffusion theory albedo boundary condition is applied. This 'penetration' calculation provides the calculation of core fuelling due to gas puffing and recycling; it also provides the albedo α_{sol} that is used in the TEP calculation of the 'outer' regions.

The total neutral source is adjusted to match the measured line averaged density when the measured confinement time is used. Gas fuelling sources, ion and neutral recycling sources, and volumetric recombination and molecular dissociation sources are represented explicitly. Additional sources, representing outgassing from the walls, are adjusted so that the line averaged density calculated by the core particle balance model from the incident neutral currents and from the internal sources due to pellet injection and neutral beam heating matches the experimental line averaged density, when the experimental value of the particle confinement time is used. Because recycling is treated explicitly, the particle confinement time is the density die-away time measured in pellet injection experiments [10], scaled in magnitude in proportion to H_{ITER89}, which in turn is adjusted to match the measured energy confinement time with the ITER-89P scaling law. Thus, the neutral modelling is adjusted to predict the correct core fuelling rate, consistent with the measured confinement time.

For the purpose of evaluating the neutral–plasma reaction rates, average neutral speeds are determined as follows. Neutrals resulting from ions or neutrals reflected as atoms from a material surface

are assigned one half the energy of the incident particle, neutrals resulting from molecular dissociation are assigned 2 eV and neutrals introduced by gas fuelling are assigned 1 eV. Neutrals are assumed to equilibrate with the local plasma temperature on the first charge exchange or elastic scattering collision (causing the plasma to lose a corresponding amount of energy). The atomic, molecular and surface data used in these calculations are discussed in Appendix B. Neutral–neutral elastic scattering is taken into account in the recycling region R.

2.2. SOL divertor plasma model

Radial transport in the SOL–divertor plasma is modelled by Bohm diffusion, leading to well known expressions for the particle and energy widths of the SOL [3]. Flux expansion in the divertor is taken into account by an experimentally determined expansion factor.

Parallel transport is modelled by 1-D density, momentum and energy equations, incident particle ($\Gamma_\perp$) and heat ($Q_\perp$) fluxes into the SOL from the core plasma, stagnation boundary conditions at the top and sheath boundary conditions at the divertor plate [3]. Radiative and ionization cooling, cooling and momentum loss due to charge exchange and elastic scattering, volumetric particle sources due to ionization and molecular dissociation and a volumetric recombination particle sink are taken into account [3]. The equations are integrated from the stagnation point at the top to the divertor plate at the bottom to obtain so-called 'two point' equations which can be solved for the plasma densities and temperatures along the separatrix at the location of the midplane and at the location of the divertor plate; intermediate values of density and temperature are obtained by interpolation, and the radial dependence is taken as exponential with the e-folding distances determined as stated in the previous paragraph. The atomic physics terms are evaluated from the neutral particle model described above and the radiation is evaluated from an integral model [11], using a coronal equilibrium fit based on the ADPAK data [12] and a non-coronal enhancement factor determined by comparison with experiment. It has been found by comparison with DIII-D experimental parameters, in several discharges, that a better match of predicted and experimental midplane temperature results when the classical Braginski parallel heat conductivity is reduced by a factor of 10.

2.3. Core plasma model

Particle and power balance models couple the core and SOL plasma models. The particle flow from the core into the SOL ($\Gamma_\perp$) is calculated to balance the net inward neutral flow plus any sources due to pellet injection and neutral beam injection. The heat flow from the core into the SOL ($Q_\perp$) is calculated to balance the total heating power plus any inflow of heat due to neutral inflow, minus the heat radiated by bremsstrahlung and impurity radiation. The latter is calculated by a coronal equilibrium fit integrated over the radial distribution.

Core transport is represented by experimental ratios, the ITER-89P scaling law and the particle confinement law [10] $\tau_n = 0.05 H_n I^2$. Experimental data for the ratios of the pedestal to line averaged densities, of the pedestal to separatrix temperatures and of the central to pedestal temperatures and densities are used as input, and the temperature and density distributions are then calculated from a 'parabola to a power on a pedestal' model. The H_{ITER89} factor is adjusted until the ITER-89P scaling law yields the experimental energy confinement time, and the particle confinement is adjusted according to $H_n = 0.9 H_{ITER89P}$. The averaged density and temperature are then calculated from $\Gamma_\perp$ and $Q_\perp$ and the appropriate confinement times.

3. Measurement and analysis of neutral density in DIII-D

A new method for measuring neutral density was recently applied in DIII-D [5]. Data from a tangentially viewing video camera were used to reconstruct the 2-D profile of D_α light intensity I_α [6]. The neutral density at the lower, or divertor, Thomson scattering location was then determined by relating the light intensity to the excitation rate per neutral atom determined from the Thomson scattering measurements of (n_e,T_e), $I_\alpha = n_0 n_e \langle \sigma(n_e, T_e) v \rangle_{exc}$. This provided measurements of the neutral density at the locations of the divertor Thomson scattering locations at 3.7–21.0 cm above the divertor floor.

A lower single null L mode discharge (shot 96740 with $I = 1.0$ MA, $B = 2.1$ T, $P_{NBI} = 0.25$ MW, $\bar{n} = 2.5 \times 10^{19}$ cm^{-3}) was run, with the X point adjusted to several different heights above the divertor floor during the course of the discharge. The divertor Thomson scattering locations were in the vicinity of the X point, such that neutral densities were measured below the X point in the private flux

region as well as above the X point inside the separatrix.

These data have been analysed previously with a coupled fluid plasma/Monte Carlo neutrals (B2.5/DEGAS) model [7]. The calculated neutral densities were in excellent agreement with the measurements above the X point in the core plasma, but the agreement deteriorated below the X point in the private flux region. This deterioration in agreement was attributed to inaccurate modelling of plasma parameters in the private flux region and to the effect of molecules in the private flux region in producing an overestimation of the experimental neutral density below the X point [7].

Using the modelling procedure outlined in Section 2, the neutral densities have been calculated for the two extreme locations of the X point for which good data were obtained — at 7 and 14 cm above the divertor floor. The calculated averaged plasma densities and electron temperatures in the edge transport barrier, which are used to model the background plasma for the neutral penetration calculations, agreed with measured values to within 5–10%.

The penetration calculation from the outside of the SOL in Fig. 1 into the core plasma was carried out for three different choices of the uncollided neutral transmission coefficient [9], $T_0 = E_2, 2E_3$ and $3E_4$, corresponding to assuming an isotropic plane source, an isotropic incident flux and a cosine incident flux, respectively, distribution for the neutrals entering from the private flux region into the SOL. Agreement of the results of these calculations with the experimental data is comparable to the agreement obtained with the Monte Carlo (B2.5/DEGAS) calculation, as shown in Figs 2 and 3.

Uncertainties in both the measurements of photon intensity and the Thomson scattering measurements of electron densities and temperatures introduce significant uncertainties into the experimental neutral densities which are inferred from them. While the uncertainties in measured neutral densities have not been analysed for the cases shown in Figs 2 and 3, uncertainties for an intermediate (in terms of X point location above the floor) case are [5] roughly (+ factor of 10, − factor of 2) above the X point and significantly larger below the X point.

The deterioration of agreement below the X point can in part be attributed to the idealized representation of the plasma below the X point as the same scrape-off layer that obtained at the plasma midplane. Measurements in DIII-D indicate that there is substantial plasma in the private flux region extending from the X point to the divertor floor. Moreover, measured data in this region have large error bars due to fluctuations in divertor Thomson scattering electron densities and temperatures and photon intensities.

4. Discussion

The good agreement between calculated and measured neutral densities above the X point indicates that the neutral penetration into the plasma core at the X point is being treated adequately by the modelling procedure outlined in Section 2. This result provides support for our previous findings [1, 2] of the importance of neutrals penetrating through the X point to the formation of MARFEs and other thermal instabilities in the edge plasma, which were based on the same neutrals modelling procedure.

The TEP [8] neutral transport method represents the recycling of neutrals to the edge plasma in terms of transport across a relatively few large regions (Fig. 1) to calculate an incident neutral flux to the edge plasma outside of the separatrix; the penetration of this incident neutral flux across the separatrix into the main plasma edge is then calculated with a spatially detailed 1-D neutral transport model. The fundamental premise of both calculations, but in particular of the large region calculation of the neutral recycling outside the main plasma, is that the transport across a region is determined primarily by the 'optical thickness' (the quantity l_i defined in Eq. (2) of Appendix A) of the mean chord length across the region, not by the detailed plasma distribution within the region. This premise, which is suggested by fundamental theoretical considerations [8, 9], would seem to be supported by the reasonably good agreement with experiment discussed above.

However, we should not take this agreement to mean that there is no need for a spatially detailed treatment of neutrals transport in the plasma edge. If a spatially detailed knowledge of the neutral particle distribution is needed, then a spatially detailed representation of neutral particle transport is required. For example, the prediction of ionization and recombination fronts or of detachment would require a detailed calculation of the neutral distribution as well as of the plasma distribution within the region such phenomena occurred. The calculational model of this article contains another example, the detailed calculation of neutral particle penetration inside the separatrix, in this case to compare with localized experimental measurements, but more generally to provide

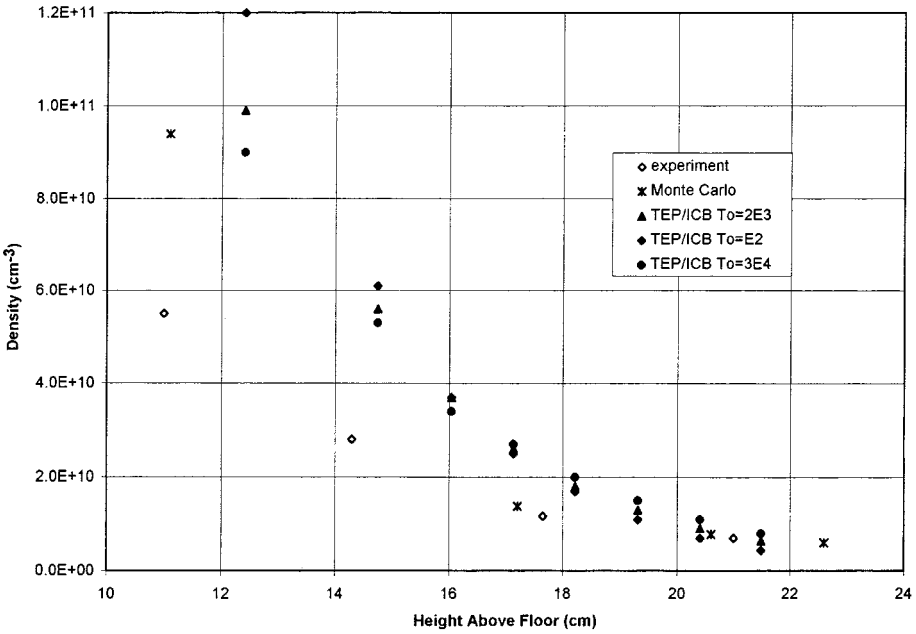

Figure 2. Measured and calculated neutral densities in the lower part of the DIII-D plasma during shot 96740 at 2250 ms when the X point was 14 cm above the divertor floor.

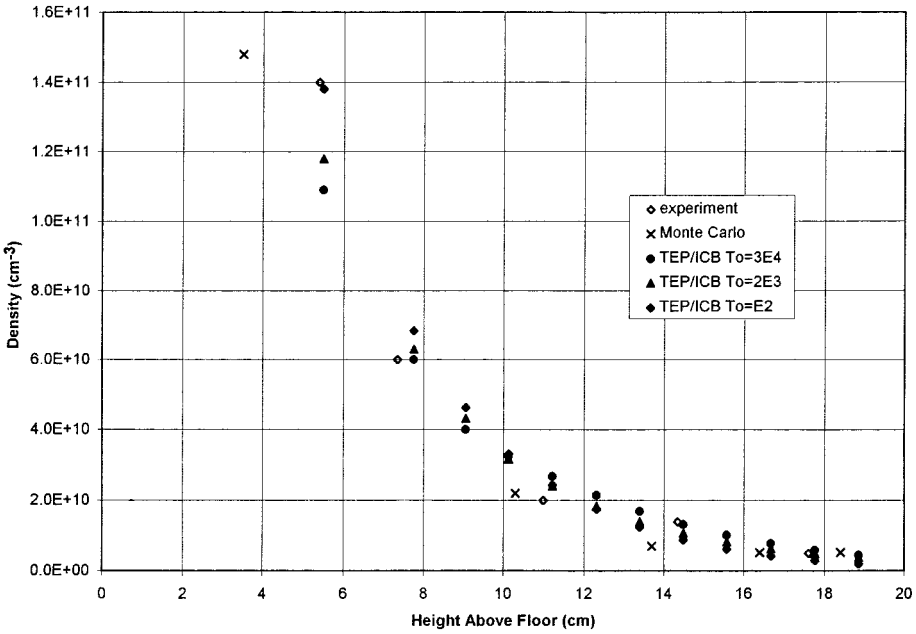

Figure 3. Measured and calculated neutral densities in the lower part of the DIII-D plasma during shot 96740 at 4250 ms when the X point was 7 cm above the divertor floor.

the local neutral density in the plasma edge for thermal instability calculations (e.g. Refs [1, 2]).

The entire iterative solution of the core plasma/SOL divertor plasma/neutrals calculation

takes less than 1 s on a modern PC. This combination of computational economy and good agreement between prediction and experiment encourages us to extend the model depicted in Fig. 1 to include:

(a) Both the inner and outer divertor channel and SOLs;
(b) More spatial detail in the neutral calculation outside the separatrix above the X point (SPL);
(c) A better treatment of the plasma in the regions (PL and PF) below the X point.

The same general modelling procedures could be applied to represent a double null divertor configuration.

It is noted that the 2-D neutrals GTNEUT code, which is based on the same TEP neutral transport methodology and which can represent the flux surface geometry of the plasma edge essentially exactly, has recently been adapted to the geometrical grid structure of the 2-D fluid edge plasma code UEDGE. The good agreement reported above supports the anticipation that, when fully coupled, the UEDGE–GTNEUT code system will provide an edge modelling capability that should be comparable in accuracy of prediction of recycling neutral penetration into the edge plasma to the presently available 2-D fluid plasma, Monte Carlo neutrals code systems, at a small fraction of the computational time.

Appendix A

A1. The ICB/TEP transport methodology

In 1-D slab geometry, the forward (+) and backward (−) partial currents at the left (i) and right ($i+1$) interfaces bounding region i are related by [9]

$$\begin{pmatrix} J_i^+ \\ J_i^- \end{pmatrix} = \begin{pmatrix} (T_i^{-1}) & (-T_i^{-1}R_i^b) \\ (R_i^b T_i^{-1}) & (T_i - R_i^b T_i^{-1} R_i^b) \end{pmatrix} \times \begin{pmatrix} J_{i+1}^+ \\ J_{i+1}^- \end{pmatrix} + \frac{1}{2}\, s_i P_i \begin{pmatrix} -T_i^{-1} \\ 1 - R_i T_i^{-1} \end{pmatrix} \qquad (1)$$

where the transport parameters are defined in terms of the exponential integral E_n

$$T_i = T_{oi} + R_i^f,\ T_{oi} = 2E_3(l_i)$$

$$R_i^{f/b} = \Lambda_i^{f/b} c_i P_i (1 - T_{oi})$$

$$P_i = \frac{P_{oi}}{1 - c_i(1 - P_{oi})}$$

$$P_{oi} = \frac{1}{2\Delta_i \Sigma_{ti}}[1 - 2E_3(l_i)]$$

$$c_i = \frac{\langle \sigma v \rangle_{cx} + \langle \sigma v \rangle_{el}}{\langle \sigma v \rangle_{ion} + \langle \sigma v \rangle_{cx} + \langle \sigma v \rangle_{el}}$$

$$l_i = \int_0^{\Delta_i} dx \Sigma_{ti}(x) \equiv \Delta_i / \bar{\lambda}_i. \qquad (2)$$

The quantities Σ_{ti}, Δ_i and λ_i are the total cross-sections for neutral–plasma reactions, the region thickness and the average mean free path, respectively, in region i. The quantity T_{oi} is the probability that a particle is transmitted across region i without a collision and $c_i(1 - T_{oi})$ is the probability that an incident particle has a scattering or charge exchange collision within the region. The quantity P_i is the probability that a neutral particle which enters region i across a given surface (i or $i+1$) and has an initial charge exchange or scattering collision within region i will eventually escape from region i after 0, 1, 2,... additional collisions. The quantities Λ_i^b and $\Lambda_i^f = 1 - \Lambda_i^b$ are the relative probabilities that the escape is across the same or opposite surface, respectively, over which the incident particle entered the region (e.g. $P_i\Lambda_i^b$ and $P_i\Lambda_i^f$ are the probabilities that a particle entering through surface i escapes through surface i and $i+1$, respectively). If the further approximations are made that scattering and charge exchange are isotropic and that the distribution of first collided, second collided, etc. particles is uniform over the region, then $\Lambda_i^f = \Lambda_i^b = \frac{1}{2}$, which is used in this article. A directionality correction factor has been developed [13].

In deriving the expression for T_{oi} it was assumed that the varying mean free path within the region could be approximated by an average mean free path for the region. The transmission probability T_o is $E_2(l_i)$ for an incident plane source, $2E_3(l_i)$ for an isotropic incident flux, $3E_4(l_i)$ for a cosine incident flux, etc. When one of the 'incident' surfaces for a region is a reflecting wall, this is modelled as a plane source of particles.

A2. The TEP methodology

The transport methodology is extended to 2-D geometry by writing the partial current out of region i into region j, J_{ij}, in terms of the incident partial currents into region i from all contiguous regions k, J_{ki}, and the 2-D extensions of the transmission and escape probabilities defined previously

$$J_{ij} = \sum_k^i T_{oi}^{kj} J_{ki} + \left[\sum_k^i \left(1 - \sum_m^i T_{oi}^{km} \right) J_{ki} \Lambda_{ij}^k \right] \times c_i P_i + s_i \Lambda_{ij} P_i. \qquad (3)$$

The transmission coefficients across region i for particles entering from region k and exiting into region j, in 2-D planar geometry with symmetry in the third dimension, are defined in terms of the Bickley functions Ki_n. The co-ordinate ξ_{ki} is along the interface between regions k and i, and $\phi_j(\xi_{ki})$ is the angle made with respect to the surface between regions k and i by a line connecting a point ξ_{ki} on that surface with a point on the surface between regions i and j

$$T_{oi}^{kj} = 2\int_{\xi_{ki}^{min}}^{\xi_{ki}^{max}} d\xi_{ki} \int_{\phi_j^{min}(\xi_{ki})}^{\phi_j^{max}(\xi_{ki})} \times \sin\phi_j \frac{Ki_3(l_i[\phi_j(\xi_{ki})])}{\xi_{ki}^{max} - \xi_{ki}^{min}}\, d\phi_j. \quad (4)$$

The escape probability can be written in terms of similar variables [13], but we choose instead to use a rational approximation of the form

$$P_{oi} = \frac{1}{x_i}\left[1 - \left(1 + \frac{x_i}{n}\right)^{-n}\right],\ x_i \equiv \frac{4V_i}{S_i\lambda_i} \quad (5)$$

where V_i and S_i are the volume (area in 2-D) and surface area (circumference in 2-D) of region i.

The rational approximation of Eq. (5) parameterizes the first flight escape probability (FFEP) in terms of the single parameter $x = 4V/S\lambda$. Although this result follows from theoretical considerations [9, 14, 15], it was confirmed [13] quite well by fitting Monte Carlo calculated FFEPs for several geometries, volume to surface ratios and values of the mean free path in terms of the single parameter x, for uniform regions.

The original Wigner rational approximation [14] ($n = 1$) is known to underestimate the FFEP in the midrange of x, and the Sauer rational approximation [15] ($n = 4.58$) has been shown to be more accurate for an infinite cylinder (circle) geometry. For uniform media, we found that [13] a new ($n = 2.09$) rational approximation agreed with Monte Carlo calculations of the FFEP to within 5% for a wide range of geometries (excluding the circle), volume to surface ratios and mean free paths, but that the Sauer approximation was superior for circular regions. Calculation of FFEPs for regions in which the plasma temperature varied by as much as a factor of 20 and the plasma temperature varied over the range 1–100 eV demonstrated [13] that Eq. (5) predicts the Monte Carlo calculated FFEP to within 5%. Equation (2) indicates that the error in total escape probability will be less than the error in the FFEP.

In the calculations of this article, the Wigner ($n = 1$) rational approximation was used. The directional escape factor, Λ_{ij}, which specifies the fraction of particles escaping from region i which enter contiguous region j, was approximated as the ratio of the length of the interface between regions i and j to the total circumference of region i.

Appendix B

Atomic and molecular data

The atomic and molecular data used in the neutral modelling procedure outlined in this article are based on the evaluation and recommendations in Refs [16–18].

B1. Ionization and recombination

The electron impact process data are based on effective rates which include stepwise events occurring via excited states and are taken from Janev et al. [19]. For neutral densities much above 10^{13} cm^{-3}, the neutral cloud becomes opaque to much of the hydrogen radiation because of resonance absorption, which alters the relative population of excited states and the effective rates of ionization and recombination. This opacity effect is only important in the recycling region in front of the divertor plate. Weissheit [20] has estimated effective rates for the situation of total opacity, in which the Lyman α transitions are fully suppressed; the recombination rates are little changed but the ionization rates are generally increased at lower electron densities from the value for higher electron densities. The degree of opacity must be calculated in order to determine the correct ionization rate in the small recycling region at the divertor plate, and that capability is not yet included in the modelling procedure of this article. Thus, the unsuppressed rates [19] are also used in the recycling region, which leads to an underprediction of local ionization for very high neutral densities; this is not a problem for the DIII-D shot 96740 analysed in this article.

B2. Charge exchange

The charge exchange data are taken from Ref. [21].

B3. Elastic scattering

Elastic scattering rates have been estimated [17, 18] from the semiclassical calculations of Schultz et al. [22] which predict cross-sections that are a factor of 2–10 higher than the widely used cross-sections

based on the classical calculations of Reiter [23]. The calculations of Schultz et al. include quantal effects which have been checked against full quantal calculations and therefore should be more accurate than the classical Reiter calculations. The rates based on the calculations of Schultz et al. are used in the modelling procedure of this article for neutral-atom–ion collisions. The cross-sections used for atom–atom collisions are an order of magnitude lower.

B4. Atomic reflection and molecular re-emission

The fraction of incident ions and neutrals which are reflected, R_N, as atomic neutrals is based on the data of Thomas et al. [24, 25]. A fraction 1-R_N of the incident particles is re-emitted as molecules. These coefficients are calculated for various wall surfaces as a function of the temperature of the Maxwellian distribution of incident particles. For $T_{in} \leq 10$ eV, $R_N = 0.18$, 0.33 and 0.76 for Be, C and W, respectively, and for $T_{in} \geq 100$ eV, $R_N = 0.09$, 0.18 and 0.60 for Be, C and W, respectively.

B5. Molecular data

The data for ground state D_2 molecules and for a single effective excited molecular state discussed in Ref. [17, 18] are used to construct effective dissociation and excitation rates for ground state molecules. The ground state dissociation/excitation rates (m^3/s) used are $3.0 \times 10^{-17}/7.0 \times 10^{-18}$ for $T_{plasma} \leq 1$ eV, $9.1 \times 10^{-15}/3.5 \times 10^{-17}$ for $T_{plasma} =$ 10 eV and $5.2 \times 10^{-14}/1.3 \times 10^{-17}$ for $T_{plasma} \geq$ 100 eV.

Molecules in the ground and excited states are assumed to dissociate before leaving the recycling region via a number of channels, including for the excited state the formation of a negative ion which is assumed to immediately combine with a plasma ion to form two neutral atoms. The numbers of neutral atoms formed by the dissociation of a ground state D_2 molecule are 1.77 for $T_{plasma} \leq 1$ eV, 1.44 for $T_{plasma} = 10$ eV and 1.0 for $T_{plasma} \geq 100$ eV. The numbers of neutral atoms formed by the dissociation of an excited state D_2 molecule are 3.0 (1 directly plus 2 via the recombination of a negative ion with a plasma ion) for $T_{plasma} \leq 1$ eV, 1.65 for $T_{plasma} = 10$ eV and 1.0 for $T_{plasma} \geq 100$ eV. The net number of ions formed per dissociation is just 2.0 minus these values.

The explicit treatment of excited molecules has been found [26] to be important in the immediate vicinity of the recycling surface but to have very little effect on the solution at some distance removed therefrom. Accordingly, only the recycling of ground state molecules was considered in the present analysis.

Acknowledgements

The author is grateful to R.J. Colchin and R. Maingi for providing the data and results of Monte Carlo calculations used in this article prior to publication and for helpful discussions of their work. This work was performed under USDOE Grant No. DE-FG02-99-ER54538 with the Georgia Tech Research Corporation.

References

[1] Stacey, W.M., Mahdavi, M.A., Maingi, R., Petrie, T.W., Phys. Plasmas **6** (1999) 3941.
[2] Stacey, W.M., Petrie, T.W., "The role of edge thermal instabilities in limiting the density in DIII-D", in preparation.
[3] Stacey, W.M., Phys. Plasmas **5** (1998) 1015.
[4] Stacey, W.M., Phys. Plasmas **5** (1998) 3656.
[5] Colchin, R.J., Nucl. Fusion **40** (2000) 175.
[6] Fenstermacher, M.E., et al., Rev. Sci. Instrum. **68** (1997) 2974.
[7] Maingi, R., et al., "Modeling 2D neutral density measurements in DIII-D", in Controlled Fusion and Plasma Physics (Proc. 26th Eur. Conf. Maastricht 1999), Vol. 23J, European Physical Society, Geneva (1999) paper P1.056.
[8] Stacey, W.M., Mandrekas, J., Nucl. Fusion **34** (1994) 1385.
[9] Stacey, W.M., Phys. Plasmas **4** (1997) 179.
[10] Maingi, R., et al., Phys. Plasmas **4** (1997) 1782.
[11] Lackner, K., Schneider, R., Fusion Eng. Des. **22** (1993) 107.
[12] Hulse, R., Nucl. Technol./Fusion **3** (1983) 259.
[13] Stacey, W.M., Mandrekas, J., Rubilar, R., "Interface current integral transport methods for the calculation of neutral atom transport in the edge region of fusion plasmas", in preparation.
[14] Wigner, E.P., et al., J. Appl. Phys. **2** (1955) 257.
[15] Sauer, A., Nucl. Sci. Eng. **16** (1965) 260.
[16] Stacey, W.M., Thomas, E.W., Evans, T.M., Phys. Plasmas **2** (1995) 3740.
[17] Thomas, E.W., Stacey, W.M., Phys. Plasmas **4** (1997) 1015.
[18] Thomas, E.W., Stacey, W.M., Phys. Plasmas **4** (1997) 678.
[19] Janev, R.K., et al., J. Nucl. Mater. **121** (1984) 10.
[20] Weissheit, J., J. Phys. B: At. Mol. Phys. **8** (1975) 2556.

[21] Barnett, C.F., Collision of H, H_2, He and Li Ions with Atoms and Molecules, Document No. DE91000527, National Technical Information Service, Springfield, VA (1990).
[22] Schultz, D.R., Ovchinniko, S.Yu., Passovets, S.V., in Atomic and Molecular Processes in Magnetic Fusion Edge Plasmas (Janev, R.K., Ed.), Plenum Press, New York and London (1994).
[23] Reiter, D., in Atomic and Molecular Processes in Controlled Thermonuclear Devices (Janev, R.K., Drawin, H.W., Eds), Elsevier, Amsterdam and New York (1993).
[24] Thomas, E.W., Janev, R.K., Smith, J., J. Nucl. Instrum. Methods B **69** (1992) 427.
[25] Thomas, E.W., Janev, R.K., Smith, J., Particle Reflection from Surfaces — A Recommended Data Base, Rep. INDC(NDS)-249, IAEA, Vienna (1994).
[26] Stacey, W.M., Thomas, E.W., "Sensitivity of predicted tokamak physics parameters to divertor atomic/molecular data and modelling", in preparation.

(Manuscript received 1 November 1999
Final manuscript accepted 22 February 2000)

E-mail address of W.M. Stacey:
weston.stacey@me.gatech.edu

Subject classification: I1, Tm